Onset and Saturation of the Kink Instability in a Current-Carrying Line-Tied Plasma

W. F. Bergerson, C. B. Forest,* G. Fiksel, D. A. Hannum, R. Kendrick, J. S. Sarff, and S. Stambler

Department of Physics, University of Wisconsin, 1150 University Avenue, Madison, WI 53706, USA

(Received 1 August 2005; published 4 January 2006)

An internal kink instability is observed to grow and saturate in a line-tied screw pinch plasma. Detailed measurements show that an ideal, line-tied kink mode begins growing when the safety factor $q = \frac{4\pi^2 r^2 B_z}{\mu_0 I_p(r) L}$ drops below 1 inside the plasma; the saturated state corresponds to a rotating helical equilibrium. In addition to the ideal mode, reconnection events are observed to periodically flatten the current profile and change the magnetic topology.

DOI: 10.1103/PhysRevLett.96.015004 PACS numbers: 52.55.Tn, 52.35.Vd, 52.72.+v

Magnetohydrodynamic (MHD) instability of current-carrying plasmas is a topic of importance to astrophysical and laboratory plasmas. In the Sun, current driven MHD instability is believed responsible for solar flares. The twisting of coronal loops caused by vortices in the photosphere results in current flow parallel to the magnetic fields. When the current exceeds a critical value dependent upon the background magnetic field, instability can occur. A considerable theoretical effort has been made to understand the instability onset by modeling these plasmas as line-tied cylindrical plasmas [1–4]. Laboratory plasmas, such as the tokamak, reversed field pinch, and spheromak, are all susceptible to kink instabilities from the same excessive twisting in field lines. In the tokamak, when the current in the plasma exceeds a critical value, the plasma deforms into a helical structure which grows exponentially on a time scale related to the time it takes an Alfvén wave to propagate across the plasma.

The stability condition depends in part upon the boundary conditions in the axial direction. For periodic boundary conditions (appropriate to toroidal plasmas) Kruskal and independently Shafranov [5,6] (hereafter referred to as KS) discovered that the condition for stability is that the safety factor $q_a \equiv \frac{aB_z}{RB_\theta(a)} > 1$, where a is the radius of the plasma, B_z is the axial magnetic field, $B_\theta(a)$ is the poloidal magnetic field generated from the current flowing in the plasma, a is the minor radius of the plasma column, and R is the major radius of the toroidal plasma. In periodic systems, the theory was extended in several ways. First, it was found that a fast growing external kink becomes unstable whenever the value of q_a is just below a low order rational value $q_a \lesssim \frac{m}{n}$ [7,8]. Second, the plasma can become unstable when the safety factor drops below 1 somewhere inside the plasma (in this case the boundary of the plasma may not move at all and the mode is classified as an internal kink mode). Finally, finite plasma resistivity can lead to the phenomenon of reconnection. In periodic systems, resistive instabilities occur at resonant surfaces where the wave number of the MHD instability is locally parallel to the equilibrium magnetic field [9].

While kink instability theory has been quite successful in predicting the behavior of toroidal plasmas, it has not been as thoroughly tested in cylindrical geometries for which the boundary conditions are modified due to line tying in highly conducting end plates. By line tying we mean that the plasma is constrained to be stationary at the ends of the cylinder due to the presence of a conducting surface. In the line-tied pinch geometry the safety factor q still governs stability, albeit with a definition of q appropriate for finite length cylindrical plasmas:

$$q(r) = \frac{4\pi^2 r^2 B_z}{\mu_0 I_p(r) L}, \tag{1}$$

where the radius of the plasma is given by r, $I_p(r)$ is the plasma current inside radius r, and L is the length of the plasma. If the plasma has uniform current density, line-tied plasmas can be analytically shown to be unstable to an external kink when $q_a < 1$ [10–12].

For nonuniform current profiles, the stability analysis is more complicated and depends upon the details of the equilibrium. Several authors have performed numerical simulations of the line-tied kink mode through the linear growth phase and followed it into the nonlinear saturated phase [3,4,13]. The numerical results are consistent with the requirement that q drop below one somewhere in the plasma, and they show that the plasma tends to kink into a knotlike instability halfway between the conducting plates. If $q < 1$ everywhere, the entire column distorts into helical external kink. If q is only below one in the central part of the plasma, an internal instability results with formation of current singularities and ultimately reconnection at the $q = 1$ radius [4,14]. The reconnection in the line-tied plasmas occurs in spite of the fact that there are no resonant surfaces.

Initial screw pinch experiments (typically short pulse experiments in which current and plasma were formed by discharging a capacitor between a simple cathode and anode) did not have the luxury of drawing upon recent advances in line-tied theory. Nonetheless, KS theory has proven robust enough to maintain applicability to nontoroidal geometries [for example see [15,16]]. The adjustable current and density profiles, described below, are a novel addition to screw pinch experiments.

In this Letter, the kink mode in a linear screw pinch is observed in a device recently constructed for studying the effects of different boundary conditions on ideal MHD activity. Clear evidence for an ideal phase (an internal kink governed by q dropping below 1), and a resistive phase with a current redistribution and reconnection, are presented. The plasma production and lifetime are long compared to the growth time of the instabilities, allowing detailed measurements of the kink mode onset at marginal stability.

The experiment (shown in Fig. 1) is 1.2 m long and has a plasma radius which can be varied from 3 to 10 cm. The vessel wall surrounding the plasma is a Pyrex glass tube with a 10 cm inner radius. A steady-state axial field, adjustable to 1000 G, is generated by four solenoidal magnets. The axial field for the plasmas described in this Letter were between 250 and 400 G. The plasma is produced by 19 electrostatic plasma guns [17] packed in a hexagonal array, seen on the right side in the figure. The plasma has an electron density of $\approx 4 \times 10^{13}$ cm^{-3} (see profile in Fig. 5) and an electron temperature of ≈ 2 ev. The size of the plasma and current profile from a single gun has been measured to have a Gaussian profile with a half maximum radius of approximately 2 cm; the gun-to-gun spacing is 3.5 cm thus providing a current source which varies by less than 25%. There is also expected to be an additional merging of the current filaments, such as that observed in Refs. [18] and simulated in [19] to smooth out the azimuthal variation of the current profile. By controlling which guns are energized the plasma size and density profile can be varied. Plasmas formed by the central seven guns are about 6 cm in radius, while a full plasma with 19 guns corresponds to a radius of 9 cm. Biasing the plasma guns with respect to the anode at the opposite end of the chamber generates an adjustable current; hence, the plasma guns can be individually adjusted for desired current profiles. A conducting plate surrounding the gun nozzles, and the conducting anode at the opposite end of the plasma, are expected to create line-tying boundary conditions for pulse lengths less than 200 ms.

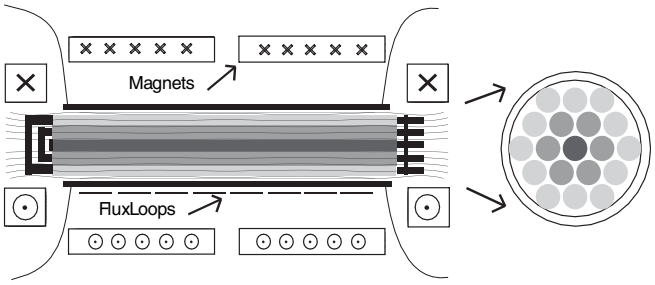

FIG. 1. A schematic of the line-tied pinch experiment. The solenoidal magnets produce a nearly uniform magnetic field between the two ends. The anode plate is on the left and drawn to highlight its the electrical connectivity. The hexagonally packed cathode array of plasma guns (shown on the right) breaks into three independently controllable regions of plasma represented by shadings in gray. The flux loops are shown in relation to the machine.

The q profile is determined by measuring the plasma current profile at the anode. The anode end plate is segmented into three concentric rings to measure the current profile (outer radii of 0.023, 0.052, and 0.081 m, respectively). By measuring the current flowing to each section, a q profile can be determined directly from Eq. (1). The MHD activity is monitored by 80 flux loops, each 6.5 cm by 12.5 cm, outside the vacuum vessel. The array is 8 (axial) $\times$ 10 (poloidal) and measures the full two-dimensional structure of $B_r(r = a, \theta, z, t)$ at the plasma boundary. The signals from the flux loops and Rogowski coils used for monitoring currents undergo analog integration prior to digitization. The plasma density profile is measured at the anode and cathode ends by a radially inserted Langmuir probe.

The majority of the data presented here is for plasmas created by the central seven guns, each gun injecting the same plasma current (less than a 10% variation between guns). The time history of a typical plasma is seen in Fig. 2. The gun arc begins at $t = 0$ ms, with the bias for the plasma current beginning at $t = 1$ ms and lasting for 8 ms. The ramp-up of the current in Fig. 2(a) corresponds to the q profile dropping in Fig. 2(b). The abrupt changes in the q profile and current traces from the segmented anode are solely a result of plasma dynamics; external conditions are unchanged throughout the plasma pulse. Figure 2(c) shows B_r from a flux loop near the center of the plasma. Strong MHD begins when q_2 drops below 1 and saturates in a millisecond.

The evolution of the MHD activity (shown in Fig. 3) prior to saturation shows that a $m = 1$ kink mode begins to grow when q drops below 1 at the center of the plasma. Figure 3(c) shows the amplitude of the poloidal mode $m =$

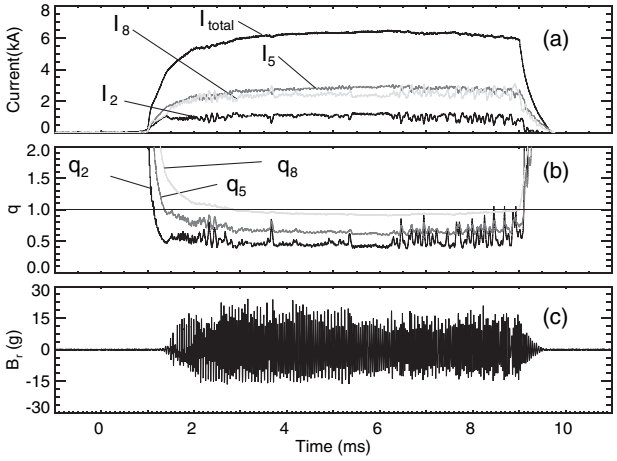

FIG. 2. The current flowing to each segment of the anode (light gray, gray, black correspond to measurements at $r = 8.1$, 5.2, and 2.3 cm, respectively) as well as total current ($B_z = 350$ Gauss). The values of q at the three radii corresponding to (a) are shown in (b). B_r as measured by integrating the voltage from a external flux loop is plotted in (c).

1 from one band of 10 flux loops at fixed axial location. The sinusoidal variation in Fig. 3(b) reflects plasma rotation, and the envelope highlights the growth of the mode. The mode begins to grow when $q_0 = q(r = 0) \cong 1$ (the gun current profiles are peaked, and so $q_0 \lesssim q_2$).

The growth rate is not accurately represented by a single number due to the increasingly unstable equilibrium current profiles. If the equilibrium is static, the amplitude should grow according to $e^{\gamma t}$. The straight dashed line in Fig. 3(c) (corresponding to $\gamma = 10.22 \times 10^3$ sec^{-1}) is a good fit only after 1.7 ms. Between 1.2 ms and 1.7 ms the growth rate is smaller as the plasma is only marginally unstable. It can be shown that if the plasma equilibrium changes slowly with time, the mode amplitude grows according to $e^{\bar{\gamma}(t)^{3/2}}$ [20]; the $\bar{\gamma}(t)^{3/2}$ dependence fits the data throughout the growth phase, with $\bar{\gamma} = 6.31 \times 10^3$ sec$^{-2/3}$.

The eigenmode grows and then saturates in the form of a rotating, helical equilibrium plasma. Figure 4 shows the frequency spectrum of a B_r trace with no relaxation activity in Fig. 4(a), while in Fig. 4(b) the plasma is undergoing many reconnection events (further discussion below). Figures 4(c) and 4(d) show $B_r(z, \theta = \text{const})$ profiles along the machine axis stepped a half period in time. The peak in Figs. 4(a) and 4(b)at 25 kHz represents the rotation of the mode which is consistent with the $\boldsymbol{E} \times \boldsymbol{B}$ rotation from a radially varying plasma potential, due to the biasing of the plasma guns that drives the current. The mode in Fig. 4(a) and 4(c) is consistent with an ideal kink being line tied at the conducting ends of the plasma.

In addition to the ideal kink mode, there is also evidence for abrupt current profile relaxation. This behavior is most easily identified as the spikelike waveforms on the q profile evolution, and can occur as discreet events (such as the event at 3.7 ms in Fig. 2), or occur periodically at a regular frequency (such as the phase between 6 and 9 ms). Figure 5 shows profiles of the current density and q before and after a relaxation event (as measured directly by the anode rings). The relaxation causes the current density to decrease near the center of the plasma while increasing at the edge. Hence q flattens and approaches 1 throughout the central plasma. Note that the reconnection time for the scale lengths of the experiment is less than 5–10 μs, short compared to all other times seen in the experiment.

The magnetic fluctuations associated with the relaxation events are not consistent with the eigenmode structure of a line-tied ideal kink mode. This is most easily seen by examining the frequency spectrum in the presence or absence of relaxation. Without relaxation, a single, monochromatic mode is observed at high frequencies [Fig. 4(a)], while in the presence of periodic relaxation, a low frequency mode appears with an amplitude that is small near the cathode end but large at the anode end of the machine seen in Fig. 4(d). The large fluctuations at the anode end can only occur if the plasma topology changes. Ideal MHD activity preserves the mapping of current from the cathode end to fixed points on the anode end, while resistive reconnection within the plasma allows the mapping to be broken [see arguments in Ref. [4,21]]. The current source, which is fixed in space at the location of the plasma guns, exits the plasma at the anode end at a different radius and poloidal location when reconnection occurs, resulting in the large low frequency fluctuations at the anode end in conjunction with relaxation events.

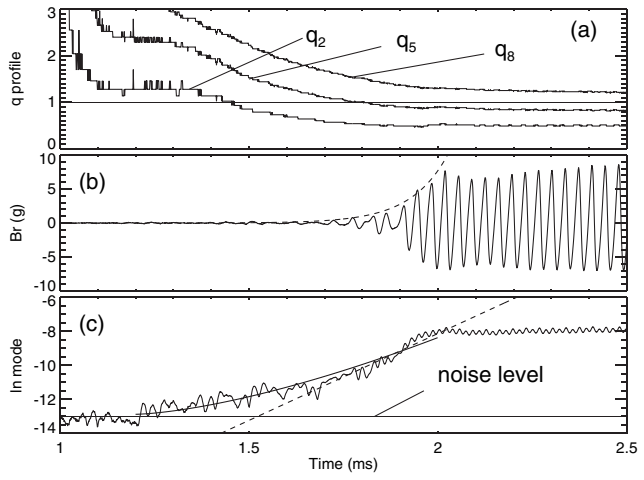

FIG. 3. (a) q profile evolution near marginality ($B_z =$ 270 Gauss). (b) The time history of B_r for a single flux loop and the best fit exponential. In (c) the logarithm of the $m = 1$ mode amplitude is plotted with an $e^{\gamma t^{3/2}}$ curve and the simple exponential. The horizontal line across the bottom in (c) is the noise level of the signal and indicates that the mode first becomes detectable at 1.22 ms.

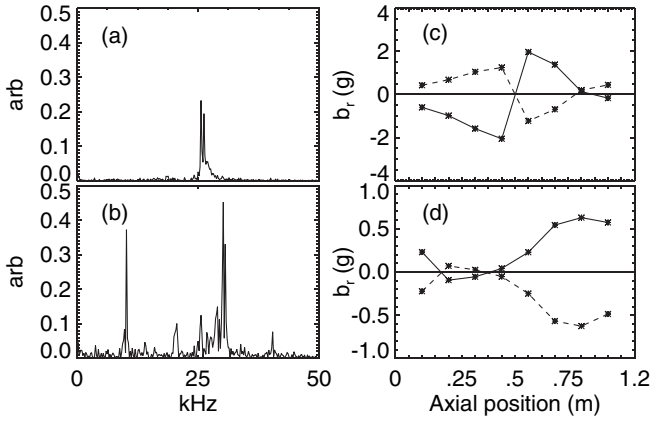

FIG. 4. In (a) [$B_z = 270$ Gauss, $I = 5000$ amps] and (b) [$B_z = 270$ Gauss, $I = 7000$ amps] the frequency spectrum of a single flux loop from the saturated phase with and without reconnection. The spectra are taken for a time interval from 5 to 9 ms and correspond to the saturated phase. In (c) and (d) the solid and hashed lines are the instantaneous axial profiles of B_r at fixed poloidal angle, band pass filtered, and then plotted at two different times separated by half a period. The standing wave structure shown in (c) corresponds to the mode at 25 kHz in (a), while the non-line-tied mode in (d) corresponds to the 10 kHz mode in (b).

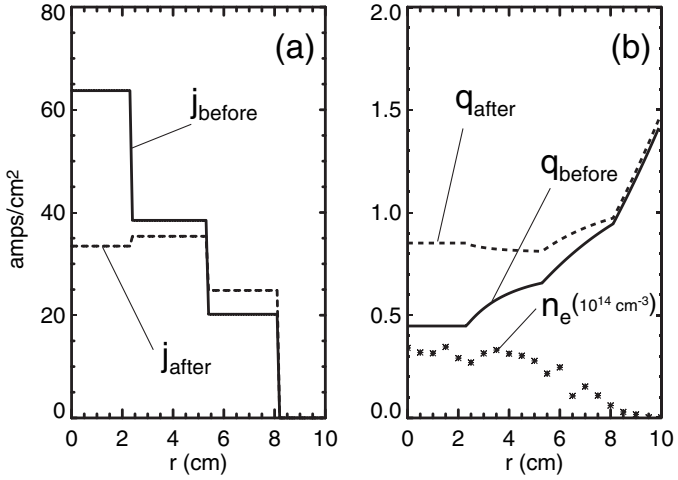

FIG. 5. (a) The current density measured by the segmented anode (solid and dashed lines correspond to before and after the relaxation event at 3.7 ms in Fig. 2). (b) The q profile corresponding to the current density is plotted along with the density profile as measured by a Langmuir probe.

The experimental observations described in this Letter are consistent with published numerical calculations [3,4,13]. The current density grows in the center of the plasma, causing the q profile to drop to 1 at that region. At that time, an ideal, internal kink begins to slowly grow and is barely detectable on the external flux loop array. Figure 3(b) shows the amplitude early on is just above the noise floor. We note that surrounding the 7 gun, current-carrying plasma described above with additional plasma (without current) from the outer 12 plasma guns greatly reduces the amplitude of the magnetic fluctuations measured at the surface of the plasma. This is consistent with the B_r eigenfunction of the internal kink mode being attenuated by the external plasma. We have noted the importance of the time-dependent equilibrium on the growth rate; as the current peaks the internal kink becomes more unstable, and the growth rate of the mode increases. The amplitude of the internal kink grows, eventually distorting the entire plasma column into a lower free energy helical equilibrium. As the helical distortion grows, the growth rate of the ideal mode eventually decreases to zero, resulting in a rotating, stationary state.

The growth rates are considerably slower than Alfvénic ($\gamma_A = V_{\text{Alfvén}}/2\pi L \approx 2 \times 10^5\ \text{sec}^{-1}$ for these plasmas), the characteristic growth rate predicted by analytic theory for the external kink in line-tied plasmas (and simple current profiles) [10–12], but are consistent with those presented in the numerical calculations modeling the internal kink. Numerical calculations of the growth rates for the profiles measured in the experiment have not yet been done, but the growth rates calculated in the numerical papers are consistent with the experimental measurements (typically 1/20th of the Alfvén transit frequency).

In summary, an ideal internal kink and a resistive MHD instability have been observed in line-tied plasmas. The reconnection events observed in the experiment show behavior which is similar in many ways to that observed in toroidal experiments. However, it is important to note that the line-tying configuration does not allow resonant magnetic surfaces where reconnection occurs in toroidal devices. Similar phenomena may have been observed in numerical simulations [e.g., those of Amo *et al.* [3]]. Measurement of the radial profile of the eigenmode (and potentially current sheets) associated with the reconnection, together with an identification of the trigger mechanism for the reconnection, remains a topic for further investigation.

The authors wish to express their thanks to Chris Hegna, Carl Sovinec, Ellen Zweibel, Stewart Prager, and Vladimir Mirnov for numerous discussions concerning kink modes in line-tied and periodic plasmas. This work was supported by the Department of Energy.

*Electronic address: cbforest@wisc.edu

[1] A. W. Hood and E. R. Priest, Sol. Phys. **64**, 303 (1979).
[2] M. Velli, G. Einaudi, and A. W. Hood, Astrophys. J. **350**, 428 (1990).
[3] H. Amo, T. Sato, A. Kageyama, and The Complexity Simulation Group, Phys. Rev. E **51**, R3838 (1995).
[4] R. Lionello, M. Velli, G. Einaudi, and Z. Mikic, Astrophys. J. **494**, 840 (1998).
[5] M. Kruskal and J. Tuck, Proc. R. Soc. A **245**, 222 (1958).
[6] V. Shafranov, Atomic Energy in Australia **5**, 38 (1957).
[7] V. Shafranov, Sov. Phys. Tech. Phys. **15**, 175 (1970).
[8] J. Wesson, Nucl. Fusion **18**, 87 (1978).
[9] H. P. Furth, J. Killeen, and M. N. Rosenbluth, Phys. Fluids **6**, 459 (1963).
[10] I. Lanskii and A. Shchetnikov, Sov. J. Plasma Phys. **16**, 322 (1990).
[11] D. D. Ryutov, R. H. Cohen, and L. D. Pearlstein, Phys. Plasmas **11**, 4740 (2004).
[12] C. C. Hegna, Phys. Plasmas **11**, 4230 (2004).
[13] Z. W. Ma and A. Bhattacharjee, Geophys. Res. Lett. **23**, 2955 (1996).
[14] R. Lionello, D. D. Schnack, G. Einaudi, and M. Velli, Phys. Plasmas **5**, 3722 (1998).
[15] S. C. Hsu and P. M. Bellan, Phys. Rev. Lett. **90**, 215002 (2003).
[16] D. H. Birdsall, S. A. Colgate, H. P. Furth, C. W. Hartman, and R. L. Spoerlein, Nucl. Fusion **3**, 955 (1962).
[17] G. Fiksel, A. Almagri, D. Craig, M. Iida, S. C. Prager, and J. Sarff, Plasma Sources Sci. Techn. **5**, 78 (1996).
[18] I. Furno, T. P. Intrator, E. W. Hemsing, S. C. Hsu, S. Abbate, P. Ricci, and G. Lapenta, Phys. Plasmas **12**, 055702 (2005).
[19] H. Takamaru and T. Sato, Phys. Plasmas **4**, 2845 (1997).
[20] J. D. Callen, C. C. Hegna, B. W. Rice, E. J. Strait, and A. D. Turnbull, Phys. Plasmas **6**, 2963 (1999).
[21] C. Sovinec, J. Finn, and D. del Castillo-Negrete, Phys. Fluids **8**, 475 (2001).